Human Molecular Genetics, 2016, Vol. 25, No. 3 571–583

doi: 10.1093/hmg/ddv497
Advance Access Publication Date: 8 December 2015
Original Article

ORIGINAL ARTICLE

ACTG2 variants impair actin polymerization in sporadic Megacystis Microcolon Intestinal Hypoperistalsis Syndrome

Danny Halim[1], Robert M.W. Hofstra[1,11], Luca Signorile[2], Rob M. Verdijk[3], Christine S. van der Werf[5], Yunia Sribudiani[1,†], Rutger W. W. Brouwer[6], Wilfred F.J. van IJcken[6], Niklas Dahl[7], Joke B.G.M. Verheij[5], Clarisse Baumann[8], John Kerner[10], Yolande van Bever[1], Niels Galjart[2], Rene M.H. Wijnen[4], Dick Tibboel[4], Alan J. Burns[1,11], Françoise Muller[9], Alice S. Brooks[1] and Maria M. Alves[1,*]

[1]Department of Clinical Genetics, [2]Department of Cell Biology, [3]Department of Pathology, and [4]Department of Pediatric Surgery, Erasmus University Medical Center, Rotterdam, The Netherlands, [5]Department of Genetics, University Medical Center Groningen, Groningen, The Netherlands, [6]Erasmus Center for Biomics, Erasmus University Medical Center, Rotterdam, The Netherlands, [7]Department of Immunology, Genetics and Pathology, Medical Genetics and Genomics, Uppsala University, Uppsala, Sweden, [8]Unité de Génétiqué Clinique, and [9]Biochimie Prenatalé, Hôpital Universitaire Robert Debré, Paris, France, [10]Lucile Salter Packard Children's Hospital, Stanford University, Palo Alto, CA, USA and [11]Birth Defects Research Centre, UCL Institute of Child Health, London, UK

*To whom correspondence should be addressed at: Department of Clinical Genetics, Erasmus University Medical Center, PO Box 2040, 3000CA Rotterdam, The Netherlands. Tel: +31 10 7037643; Email: m.alves@erasmusmc.nl

Abstract

Megacystis Microcolon Intestinal Hypoperistalsis Syndrome (MMIHS) is a rare congenital disorder, in which heterozygous missense variants in the Enteric Smooth Muscle actin γ-2 (*ACTG2*) gene have been recently identified. To investigate the mechanism by which *ACTG2* variants lead to MMIHS, we screened a cohort of eleven MMIHS patients, eight sporadic and three familial cases, and performed immunohistochemistry, molecular modeling and molecular dynamics (MD) simulations, and *in vitro* assays. In all sporadic cases, a heterozygous missense variant in *ACTG2* was identified. ACTG2 expression was detected in all intestinal layers where smooth muscle cells are present in different stages of human development. No histopathological abnormalities were found in the patients. Using molecular modeling and MD simulations, we predicted that *ACTG2* variants lead to significant changes to the protein function. This was confirmed by *in vitro* studies, which showed that the identified variants not only impair ACTG2 polymerization, but also contribute to reduced cell contractility. Taken together, our results confirm the involvement of ACTG2 in sporadic MMIHS, and bring new insights to MMIHS pathogenesis.

†Present address: Department of Biochemistry and Molecular Biology, Faculty of Medicine, Universitas Padjadjaran, Bandung, Indonesia.
Received: September 24, 2015. **Revised and Accepted:** November 30, 2015

Introduction

Megacystis Microcolon Intestinal Hypoperistalsis Syndrome (MMIHS) (OMIM 249210) is the most severe form of intestinal obstruction in neonates. It was first reported by Berdon *et al.* in 1976, and is characterized by non-obstructive bladder distension, microcolon and decreased or absent intestinal peristalsis (1). MMIHS is a rare congenital disorder for which surgical intervention is normally required. However, this frequently results in futile therapy without improvement of the clinical symptoms. Pathological evaluation of intestinal biopsies collected from patients has resulted in different theories regarding the underlying cause of MMIHS. Some reports suggested a muscular problem (2–4), while others stated that the main defect was neuronal with both increased and decreased numbers of neurons being detected (5–7). Abnormalities of the interstitial cells of Cajal have also been associated with MMIHS pathogenesis (8,9). However, most of these findings were obtained in one or a few number of patients using different methods, and consensus regarding pathogenesis does not exist.

Familial appearance and parental consanguinity have been previously reported for MMIHS, suggesting that it is an autosomal recessive disorder (10,11). However, since most MMIHS cases are sporadic, it seems reasonable to hypothesize that locus heterogeneity exists, and that the genetic etiology of sporadic and familial MMIHS cases may differ. Recently, this hypothesis has been confirmed by the identification of pathogenic variants in two genes: the Enteric Smooth Muscle Actin γ-2 (*ACTG2*) gene and the smooth muscle myosin heavy chain (*MYH11*) gene. Heterozygous missense variants in *ACTG2* were identified as the cause of sporadic MMIHS in three independent studies (12–14), while a homozygous missense variant in *MYH11* was identified in a newborn patient of consanguineous descent (15). *ACTG2* encodes one of the six actin isoforms present in humans and is specifically expressed in smooth muscle cells of the intestinal and urogenital tracts (12,16,17). *MYH11* encodes for the myosin heavy chain protein, one of the components required for smooth muscle contraction. Loss of *Myh11* in mice has been reported to result in a bladder and intestinal phenotype reminiscent to the one seen in MMIHS patients (18), supporting the involvement of this gene in MMIHS pathogenesis.

Interestingly, heterozygous missense variants in *ACTG2* have also been described to cause another intestinal disorder, i.e. visceral myopathy (VM; OMIM 155310). Four families were reported with heterozygous *ACTG2* variants affecting three different residues: R40 (missense), R148 (missense) and G269 (tandem base substitution) (13,19–21). Since MMIHS and VM are mainly characterized by inadequate contractility of the intestine and variable levels of bladder dysfunction (severe in MMIHS and often mild in VM), it is not surprising that the same gene is involved in the pathogenesis of both disorders. However, it raised the hypothesis that MMIHS and VM are one disease entity with different spectrums of severity.

Despite the identification of *ACTG2* as a disease-causing gene for MMIHS, it is still unclear how variants in *ACTG2* lead to its development. In this study, we confirm the involvement of *ACTG2* in MMIHS, and bring new molecular insights into the mechanism associated with the pathogenesis of this disease.

Results

Heterozygous missense variants in *ACTG2* are present in sporadic MMIHS patients

Since previous studies have implicated *ACTG2* in MMIHS development, we screened our cohort of 11 patients for the presence of variants in this gene (Fig. 1A). All patients presented with typical MMIHS features, including a microcolon and an enlarged bladder (Table 1). In all sporadic MMIHS cases, a heterozygous missense variant in *ACTG2* was identified (Table 2). In three of these cases, we were able to confirm the *de novo* status of the variants. However, for the remaining five patients, this was not possible due to unavailability of parental DNA. The missense variants identified in our patient cohort are located in three different exons of *ACTG2*, exons 3, 4 and 7 (Fig. 1B), and are all predicted to be pathogenic by at least 2 of 3 prediction programs (PolyPhen, MutationTaster and Provean) (Table 2). None of these variants are present in the 1000 Genomes project database or in the Exome Sequencing project, but all of them have been reported before in MMIHS patients (Table 2) (12–14). No variant in *ACTG2* was identified in the three familial cases (F1, F2 and F3).

ACTG2 is expressed in all smooth muscle cells during human intestinal development

Since MMIHS is an intestinal congenital anomaly, we assessed the expression of ACTG2 in the human intestine (jejunum/ileum) at weeks 9, 11 and 22 of embryonic development, and at neonatal stage. At all developmental stages, ACTG2 was abundantly expressed in the cytoplasm of smooth muscle cells, including smooth muscle cells of the muscularis mucosa, inner circular layer and outer longitudinal layer of the muscularis propria (Fig. 2A). ACTG2 expression was also detected in vascular smooth muscle cells of the intestine, and surprisingly, in myofibroblast cells of the mucosal layer. Since myofibroblasts have been described to only express the smooth muscle actin α 2 (ACTA2) (22), we cannot exclude the possibility that the antibody used recognizes both the α and γ smooth muscle actin isoforms, and could therefore, be unspecific for ACTG2.

MMIHS patients with *ACTG2* variants do not show abnormal expression of ACTG2, or primary defects in any cellular constituents of the intestine

To define the histopathological findings in MMIHS patients with an *ACTG2* variant, we investigated the expression of ACTG2, neurofilaments, ACTA2, c-Kit/CD117, and tryptase by immunohistochemistry, in intestinal material obtained from three MMIHS patients (S1, S3 and S5). Intestinal specimens collected during autopsy from an age-matched control were used for comparison. In the three patients analyzed, we were unable to detect any difference in the expression levels of ACTG2 when compared with the control (Fig. 2B). The same result was obtained for neurofilaments and ACTA2 (Fig. 2B, Supplementary Material, Fig. S1). An increased expression of c-Kit/CD117, a marker for interstitial cells of Cajal, was observed in the intestinal mucosa of Patients S1 and S3 (Fig. 2B, Supplementary Material, Fig. S1), but no change was observed in Patient S5. Considering that c-Kit/CD117 is also a marker for mast cells, a tryptase staining was performed, confirming that the increased expression of c-Kit/CD117 in these two patients was due to an increased number of mast cells.

Missense variants in *ACTG2* lead to significant changes to the protein structure

To gain a better understanding of the possible mechanisms underlying the development of MMIHS, we performed molecular modeling and molecular dynamics (MD) simulations for ACTG2. Molecular modeling involves editing protein structures by, for instance, introducing amino acid substitutions into a known

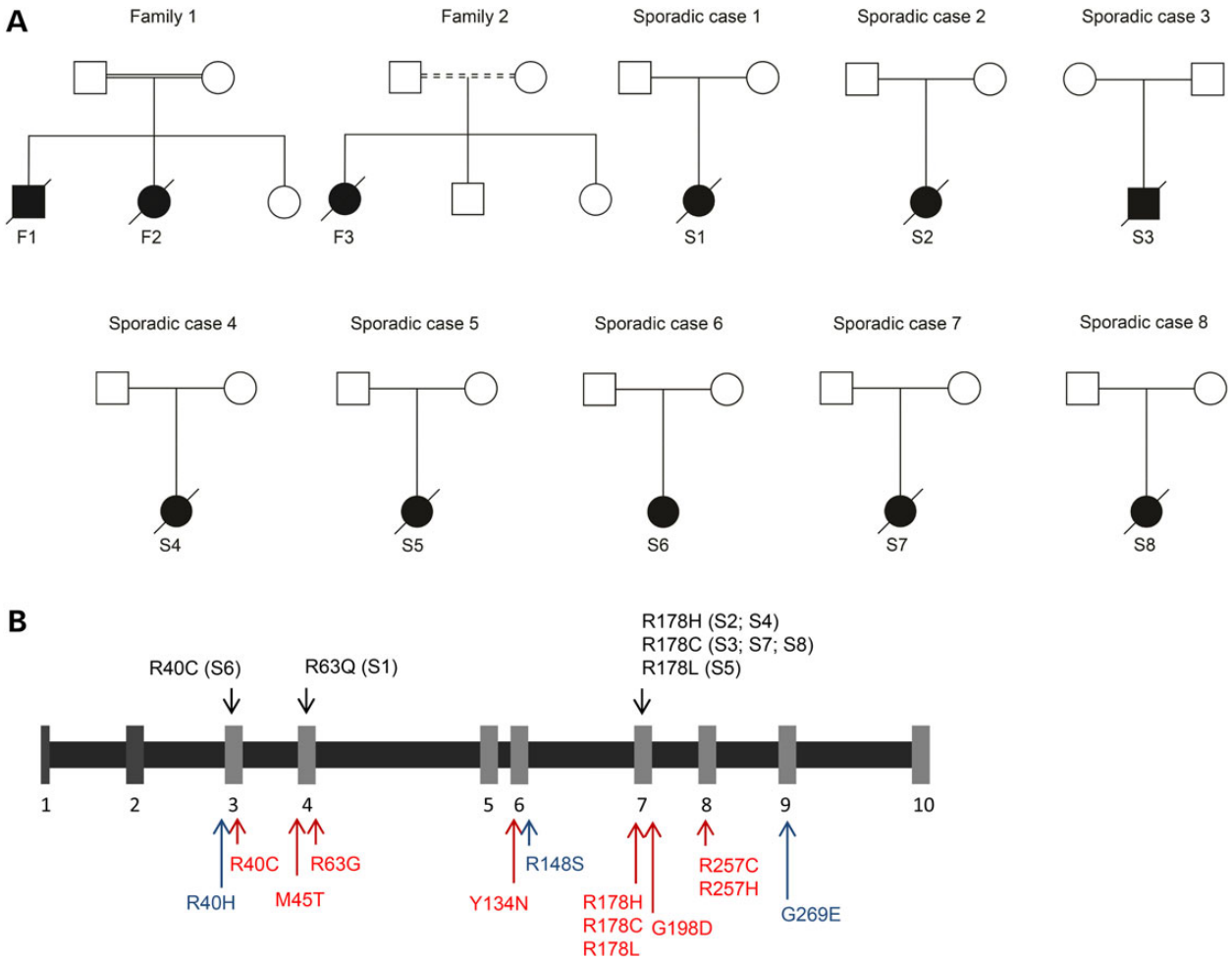

Figure 1. Analysis of *ACTG2* variants in MMIHS patients. (**A**) Pedigrees of the 10 families included in this study. (**B**) Overview of the 10 exons of *ACTG2* with all the variants identified to date. The F110L variant is not represented, as it affects an alternate exon 4 of a predicted *ACTG2* short isoform (14) (black, in this study; red, previously reported MMIHS cases; blue, identified in VM patients).

crystal structure of a protein. However, since molecular modeling is often insufficient to infer the functional role of such substitutions, MD simulations are often performed. Using this approach, the atoms of the (modeled) crystal structures are allowed to move according to the forces exerted by the surrounding environment (temperature, pressure, water, ions, nearby atoms, electrostatic interactions, hydrophobic interactions, etc.). Their motion can be measured at each time point of the simulation and followed for the entire duration of the movement. In the end, these motions are plotted as the root-mean square displacement (RMSD) from the initial crystal structure, over time. Therefore, higher RMSD values at a given time correspond to more structural differences in respect to the starting crystal structure, allowing prediction of the behavior of a (mutated) protein over time. The alpha-carbons are usually the subset of atoms chosen for such analysis. Since they represent the 'skeleton' of the protein, their motion is more restricted than the side chains, which are more likely to suffer irrelevant high deviations associated to their intrinsic flexibility. Up to date, there is no statistical test that can be performed on RMSDs to assess significant differences. However, the persistence and the extent of the differences in RMSD, coupled with visual inspection of the simulated trajectories, are used to determine the relevance of such differences.

Since the human ACTG2 structure was not available, we used in this study the chicken actin gamma monomer, which is 99.2% homologous in primary sequence (they differ only by three residue). We systematically compared the structure of the entire ACTG2 protein or its main relevant sites, for wild type (WT) and mutants during 10 ns (Tables 3–6). All mutants displayed structural differences to some extent with respect to WT ACTG2 (Fig. 3A and B). However, the most striking observations were associated with the R178C mutant, which showed the highest RMSD of the alpha-carbon trace throughout the whole simulation time for the entire protein (Fig. 3B, Table 3). We also noticed that Subdomains II and IV behaved differently from WT, since they moved closer to each other over time, instead of moving slightly apart (Fig. 3A). The average distance during the majority of the simulation time was about half compared with the WT (Fig. 3C). Distances were computed between the alpha-carbons of Thr 67 (Subdomain II) and of Ala 205 (Subdomain IV), with an average of 7.3 ± 1.5 Å for R178C and 14.2 ± 1.5 Å for the WT (Fig. 3C). The R40C mutant showed the lowest average RMSD value for the entire protein (2.536 Å compared with 2.856 Å for the WT), reflecting a less dynamic structure with respect to WT ACTG2, as well as for the ADP-ribosylation site (residues 174–182), with an average RMSD of 1.26 Å (compared with 1.82 Å for

Table 1. Clinical features of the MMIHS patients reported in this study

Patient	Consanguinity	Gender	Prenatal findings	Age of onset	Megacystis	Microcolon	Hypoperistalsis[a]	Malrotation	Performed surgeries	Additional symptoms	Outcome	Cause of death
F1	Yes	Female	Megabladder	Prenatal	+	+	+	+	None	None	Deceased	Termination of pregnancy
F2	Yes	Male	Megabladder	Prenatal	+	NA	NA	NA	None	None	Deceased	Termination of pregnancy
F3	Suspected	Female	Megabladder	Prenatal	+	+	+	+	?	None	Deceased	NA
S1	No	Female	Megabladder, hydronephrosis, hydroureter	Prenatal	+	+	+	+(volvulus at 5 y.o.)	Gastrostomy, ileostomy, small intestinal resection, entire colon resection, multivisceral organ transplantation	None	Deceased (23 y.o.)	Multiple organ failure
S2	No	Female	?	?	+	+	+	?	?	?	Deceased	?
S3	No	Male	Low urinary tract obstruction with bilateral hydronephrosis, mega-ureter, abdominal wall dehiscence	Prenatal	+	+	+	+	Laparotomy	Lax abdominal wall, undescended testis	Deceased (5 d.o.)	Discontinued treatment
S4	No	Female	Megabladder, bilateral hydronephrosis, polyhydramnios	Prenatal	+	+	+	+	Laparotomy	None	Deceased (5 m.o.)	Discontinued treatment
S5	No	Female	Megabladder, polyhydramnios	Prenatal	+	+	+	+	Laparotomy, suprapubic catheterization	None	Deceased (8 m.o.)	Multiple organ failure
S6	No	Female	Megabladder	Prenatal	+	+	+	+	Gastrostomy, ileostomy, colostomy, cholecystectomy, small intestinal resection	None	Alive (24 y.o.) with parenteral and enteral nutrition	Alive
S7	No	Female	N/A	Prenatal	+	+	?	?	None	?	Deceased	?
S8	No	Female	N/A	Prenatal	+	+	?	?	None	?	Deceased	?

[a]Detected by manometric study/barium enema; N/A, not available; ?, unknown; y.o., years old; d.o., days old; m.o., months old.

Table 2. Overview of all the *ACTG2* mutations detected in MMIHS and VM patients

Patient	Gene	Position	Exon	AA position	Effect	Polyphen	MutationTaster	Provean	*De novo*
F1	(–)								
F2	(–)								
F3	(–)								
S1	ACTG2	74129548	4	R63Q	Nonsynonymous	Probably damaging	Disease causing	Neutral	?
S2	ACTG2	74140693	7	R178H	Nonsynonymous	Benign	Disease causing	Deleterious	Yes
S3	ACTG2	74140692	7	R178C	Nonsynonymous	Benign	Disease causing	Deleterious	Yes
S4	ACTG2	74140693	7	R178H	Nonsynonymous	Benign	Disease causing	Deleterious	?
S5	ACTG2	74140693	7	R178L	Nonsynonymous	Probably damaging	Disease causing	Deleterious	Yes
S6	ACTG2	74128449	3	R40C	Nonsynonymous	Probably damaging	Disease causing	Deleterious	?
S7	ACTG2	74140692	7	R178C	Nonsynonymous	Benign	Disease causing	Deleterious	?
S8	ACTG2	74140692	7	R178C	Nonsynonymous	Benign	Disease causing	Deleterious	?
MMIHS 1[12]	ACTG2	74140693	7	R178L	Nonsynonymous	Probably damaging	Disease causing	Deleterious	Yes
MMIHS 2[12]	ACTG2	74140692	7	R178C	Nonsynonymous	Benign	Disease causing	Deleterious	Yes
MMIHS 3[13]	ACTG2	74141962	8	R257C	Nonsynonymous	Probably damaging	Disease causing	Deleterious	Yes
MMIHS 4[13]	ACTG2	74140693	7	R178H	Nonsynonymous	Probably damaging	Disease causing	Deleterious	No
MMIHS 5[13]	ACTG2	74129494	4	M45T	Nonsynonymous	Probably damaging	Disease causing	Deleterious	Yes
MMIHS 6[13]	ACTG2	74136215	6	Y134N	Nonsynonymous	Benign	Disease causing	Deleterious	Yes
MMIHS 7[13]	ACTG2	74129547	4	R63G	Nonsynonymous	Probably damaging	Disease causing	Deleterious	?
MMIHS 8[13]	ACTG2	74141962	8	R257C	Nonsynonymous	Probably damaging	Disease causing	Deleterious	Yes
MMIHS 9[13]	ACTG2	74128449	3	R40C	Nonsynonymous	Probably damaging	Disease causing	Deleterious	Yes
MMIHS 10[13]	ACTG2	74140753	7	G198D	Nonsynonymous	Probably damaging	Disease causing	Deleterious	Yes
MMIHS 11[13]	ACTG2	74140692	7	R178C	Nonsynonymous	Benign	Disease causing	Deleterious	Yes
MMIHS 12[13]	ACTG2	74141962	8	R257C	Nonsynonymous	Probably damaging	Disease causing	Deleterious	Yes
MMIHS13[13]	ACTG2	74140693	7	R178H	Nonsynonymous	Probably damaging	Disease causing	Deleterious	Yes
MMIHS 14[13a]	ACTG2	74141962	8	R257C	Nonsynonymous	Probably damaging	Disease causing	Deleterious	No
MMIHS 15[13b]	ACTG2	74129825	4[d]	F110L	Nonsynonymous	?	?	?	?
MMIHS 16[13b]	ACTG2	74129825	4[d]	F110L	Nonsynonymous	?	?	?	?
MMIHS 17[13c]	ACTG2	74128450	3	R40H	Nonsynonymous	Probably damaging	Disease causing	Neutral	No
MMIHS 18[14]	ACTG2	74141963	8	R257H	Nonsynonymous	Probably damaging	Disease causing	Deleterious	Yes
MMIHS 19[14]	ACTG2	74141963	8	R257H	Nonsynonymous	Probably damaging	Disease causing	Deleterious	Yes
MMIHS 20[14]	ACTG2	74141962	8	R257C	Nonsynonymous	Probably damaging	Disease causing	Deleterious	Yes
MMIHS 21[14]	ACTG2	74140693	7	R178H	Nonsynonymous	Probably damaging	Disease causing	Deleterious	Yes
VM 1[19]	ACTG2	74140602	6	R148S	Nonsynonymous	Probably damaging	Disease causing	Deleterious	No
VM 2[19]	ACTG2	74140602	6	R148S	Nonsynonymous	Probably damaging	Disease causing	Deleterious	No
VM 3[19]	ACTG2	74140602	6	R148S	Nonsynonymous	Probably damaging	Disease causing	Deleterious	No
VM 4[19]	ACTG2	74140602	6	R148S	Nonsynonymous	Probably damaging	Disease causing	Deleterious	No
VM 5[19]	ACTG2	74140602	6	R148S	Nonsynonymous	Probably damaging	Disease causing	Deleterious	No
VM 6[19]	ACTG2	74140602	6	R148S	Nonsynonymous	Probably damaging	Disease causing	Deleterious	No
VM 7[19]	ACTG2	74140602	6	R148S	Nonsynonymous	Probably damaging	Disease causing	Deleterious	No
VM 8[13]	ACTG2	74128450	3	R40H	Nonsynonymous	Probably damaging	Disease causing	Neutral	Yes
VM 9[20]	ACTG2	74140602	6	R148S	Nonsynonymous	Probably damaging	Disease causing	Deleterious	?
VM 10[21]	ACTG	74141999–74142000	9	G269E	Nonsynonymous	Probably damaging	Disease causing	Deleterious	No
VM 11[21]	ACTG	74141999–74142000	9	G269E	Nonsynonymous	Probably damaging	Disease causing	Deleterious	No

Table continues

Table 2. Continued

Patient	Gene	Position	Exon	AA position	Effect	Polyphen	MutationTaster	Provean	*De novo*
VM 12[21]	ACTG	74141999–74142000	9	G269E	Nonsynonymous	Probably damaging	Disease causing	Deleterious	No
VM 13[21]	ACTG2	74141999–74142000	9	G269E	Nonsynonymous	Probably damaging	Disease causing	Deleterious	No
VM 14[21]	ACTG2	74141999–74142000	9	G269E	Nonsynonymous	Probably damaging	Disease causing	Deleterious	No
VM 15[21]	ACTG2	74141999–74142000	9	G269E	Nonsynonymous	Probably damaging	Disease causing	Deleterious	No
VM 16[21]	ACTG2	74141999–74142000	9	G269E	Nonsynonymous	Probably damaging	Disease causing	Deleterious	No

?, Unknown due to unavailability of parental DNA. F, familial; S, sporadic; [a]patient with megacystis and pseudo-obstruction; [b]patient with pseudo-obstruction; [c]familial history of pseudo-obstruction and one MMIHS case. [d]Alternative exon of a predicted short ACTG2 isoform.

the WT) (Fig. 3B, Tables 3 and 5). An exception to the generally lower structural deviations of the R40C mutant was observed for the region spanning residues 357–376, which belongs to the myosin-binding site. This region showed a significant displacement, having an average RMSD of 3.557 Å in contrast with 2.383 Å for the WT (Table 6). Moreover, the region spanning residues 41–53, belonging to the D-loop, resulted in lower RMSD values for the R40C mutant (4.995 ± 1.998 Å) when compared with the WT (7.061 ± 1.077 Å, Table 4).

ACTG2 polymerization is impaired by the presence of a missense variant

To further investigate the effect of the missense variants found in MMIHS patients on the overall function of ACTG2, we determined the localization of WT and mutant proteins with phalloidin, a known marker of filamentous actin (F-actin). We over-expressed a tagged version of ACTG2 WT and mutant proteins in a human osteosarcoma cell line (U2OS), and specifically looked for co-localization between ACTG2 and actin fibers. While the WT protein could incorporate into the actin filaments, no co-localization was observed for any of the mutants analyzed (Fig. 4A). We further confirmed this finding by performing *in vitro* actin binding assays. In these assays, polymerized actin is pelleted by high-speed centrifugation, and the binding of ACTG2 to the actin filaments is determined by co-sedimentation. We found that while ACTG2 WT was able to pellet in the presence of F-actin, all the mutants analyzed remained in the supernatant both in the absence and presence of polymerized actin (Fig. 4B).

ACTG2 missense variants reduce cellular contractility

Contraction and relaxation of smooth muscles occur in an involuntary manner and are critical processes for the normal functioning of the vascular, digestive, respiratory and urogenital systems (19). ACTG2 is the main actin isoform present in visceral smooth muscle, and previous studies showed that its presence is necessary for the controlled dilatation of various muscular structures within the body (22). Recent *in vitro* studies have also reported that ACTG2 is involved in cellular contractility, and that variants in *ACTG2* lead to reduced cellular contraction (12,19). Therefore, we decided to investigate if the missense variants identified in our cohort of patients also affect cellular contractility. For that, U2OS cells were transfected with ACTG2 WT and mutant vectors, and cell contraction assays were performed *in vitro* based on the contraction of a collagen matrix. Our results showed that all missense variants analyzed affected cellular contractility (Fig. 4C), but this effect was only significant ($P < 0.05$) for the variants affecting codon 178 (R178H, R178C, R178L; Fig. 4D).

The *ACTG2* variant R148S identified in visceral myopathy leads to similar *in vitro* changes as the ones described for MMIHS

Since heterozygous *ACTG2* missense variants are also known to cause VM (13,19–21), we investigated the effect of one of these variants (R148S) on the structure and function of ACTG2. We performed molecular modeling and MD simulations, and the same set of *in vitro* assays described above for the MMIHS-associated variants. Our MD simulations showed that the R148S mutant protein behaved similarly to the WT, and we could only detect an increasing RMSD (for the entire protein trace) toward the end of the simulation (Fig. 5A). However, this increasing RMSD is likely due to the high RMSD values for the residues belonging to the D-loop

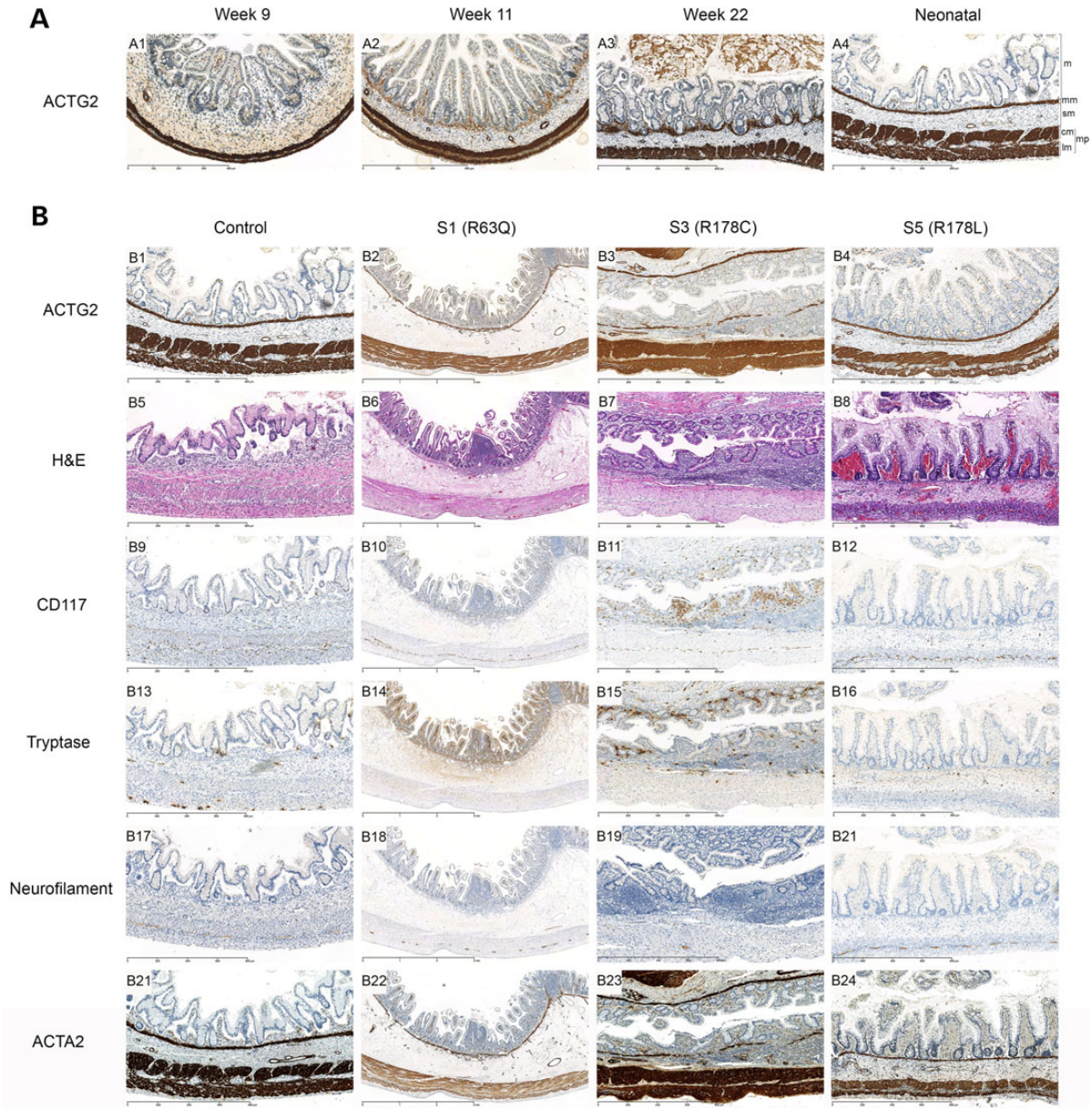

Figure 2. Expression of ACTG2 in human intestinal material. (**A**) Immunohistochemistry analysis shows that ACTG2 is expressed in the human intestine during different stages of development. (**B**) Immunohistochemistry performed in intestinal material obtained from three MMIHS patients, S1, S3 and S5, and an age-matched control shows a diffuse cellular distribution of ACTG2 in the cytoplasm of smooth muscle cells of the muscularis mucosa, blood vessels and, the circular and longitudinal muscle of muscularis propria in patients and control. No significant changes were detected in any cellular constituents of the intestine of MMIHS patients, shown by hematoxylin (HE) staining and immunohistochemistry for c-Kit/CD117, tryptase, neurofilament and ACTA2. Legends: m, mucosa; mm, muscularis mucosa; sm, submucosa; cm, circular muscle; lm, longitudinal muscle; mp, muscularis propria. Scale bars: 400 µm in A1; 600 µm in A2; 800 µm in A3, A4, B1, B3, B4, B5, B7, B8, B9, B11, B12, B13, B15, B16, B17, B19, B20, B21, B23, B24; 3 mm in B2, B6, B10, B14, B18, B22.

Table 3. RMSD value for ACTG2 WT and mutant proteins

ACTG2 (376 residues)		
ACTG2	Average (Å)	SD
WT	2.856	0.288
R178C	3.476	0.448
R178L	2.779	0.361
R178H	3.168	0.363
R40C	2.536	0.343
R63Q	2.815	0.255
R148S	3.079	0.429

Table 4. RMSD value for the D-loop in ACTG2 WT and mutant proteins

D-loop (residues 41–53)		
ACTG2	Average (Å)	SD
WT	7.061	1.077
R178C	8.405	1.697
R178L	6.376	1.447
R178H	8.012	1.488
R40C	4.955	1.998
R63Q	8.055	1.180
R148S	9.455	2.320

Table 5. RMSD value for the ADP-ribosylation site in the ACTG2 WT and mutant proteins

ADP-ribosylation site (residues 174–182)		
ACTG2	Average (Å)	SD
WT	1.820	0.545
R178C	2.106	0.454
R178L	1.996	0.545
R178H	1.712	0.340
R40C	1.260	0.338
R63Q	1.856	0.381
R148S	1.350	0.240

Table 6. RMSD value for the myosin-binding site in the ACTG2 WT and mutant proteins

Myosin-binding site (residues 357–376)		
ACTG2	Average (Å)	SD
WT	2.383	0.636
R178C	2.564	0.361
R178L	2.328	0.407
R178H	2.630	0.517
R40C	3.557	0.506
R63Q	2.560	0.716
R148S	2.827	0.440

(9.455 Å for the R148S variant in comparison with 7.061 Å for the WT, Table 4), an intrinsically flexible region. Exclusion of the D-loop from the analysis gave RMSD values for the entire R148S mutant protein comparable with the ones obtained for the WT and the R40C mutant (data not shown). The analysis of the 10 ns simulation also showed that the R148S variant led to specific structural modifications of the ACTG2 protein that are comparable with the R40C variant. Both these mutant proteins showed the lowest RMSD average values at the ADP-ribosylation site (1.260 and 1.350 Å for the R40C and R148S variants, respectively), which reflect a less dynamic structure when compared with the WT (1.820 Å) (Table 5). They also presented the highest alpha-carbon trace displacements at the myosin-binding site (3.557 and 2.827 Å for the R40C and R148S, respectively) when compared with the WT (2.383 Å, Table 6), suggestive of structural differences at this site that could possible translate into suboptimal interactions with myosin. Our *in vitro* assays also showed that, similarly to what we observed for the MMIHS variants, the cellular localization of ACTG2 is disrupted by the presence of the R148S variant, as well as its ability to bind to actin filaments (Fig. 5B and C). Moreover, a reduction in cell contractility was detected in the presence of this variant, as previously described (Fig. 5D and E) (19).

Discussion

ACTG2 is the main actin isoform expressed in intestinal smooth muscle cells, and it is therefore, not surprising that changes affecting its structure lead to severe disruption of normal intestinal development and function. Recently, heterozygous *ACTG2* variants have been identified as the cause of MMIHS (12–14). In this study, we confirm the involvement of ACTG2 in this disorder, and show that the heterozygous missense variants associated with MMIHS are pathogenic, disrupting actin polymerization. As a consequence, cellular contractility is affected, which could account for the phenotypic abnormalities seen in MMIHS patients. Surprisingly, no differences in the expression levels of ACTG2, or any other major histological abnormalities, were detected in the intestinal biopsies of MMIHS patients, despite previous studies have reported pathological abnormalities associated with this disorder (2–9). However, since most of these studies did not provide a genetic etiology for the patients reported, and some abnormal findings, such as an increased number of mast cells, can be a secondary effect due to reactive changes normally associated with bowel obstruction, the use of histological analysis for diagnostic purposes still needs to be carefully evaluated. Of particular notice is a recent report describing differences in ACTG2 expression between one MMIHS patient carrying a R178H variant and a control (14). In our study, two patients with a variant on the same codon were also analyzed immunohistochemically (Fig. 2B, Patients S3 and S5), but we were unable to find any differences when compared with the control. Although we find this discrepancy difficult to explain, we believe that the sample size in both cases is rather small and thus, any inferences must be treated with caution.

To date, all *ACTG2* variants associated with MMIHS affect specific residues strongly conserved among different species (Table 2) (12–14). There also seems to be an over-representation of variants associated with residue 178 in MMIHS (Fig. 1B, Table 2), which is suggestive of a possible mutational hotspot in this region. Since no clear loss of function variants (early stop codons or out of frame insertions/deletions) have been identified in any of the MMIHS patients reported, and no difference in ACTG2 expression levels has been found in patients and controls (Fig. 2B), we hypothesize that the variants identified in *ACTG2* are likely to have a dominant negative effect. Based on our functional studies, we cannot establish a genotype–phenotype correlation, since all the variants seem to behave in a similar way. However, considering that in our cohort, patients with a variant in residue 178 died a few days after birth, and the only patient alive has a R40 variant (S6), it is tempting to speculate that variants affecting residue 178 have a stronger dominant effect leading to a more severe phenotype. Interestingly, residue 178 of ACTG2 corresponds to residue 179 of ACTA2, which has been reported to be mutated in patients diagnosed with early-onset vascular disease associated with smooth muscle cell dysfunction (23), and in a patient with prune belly syndrome (24), supporting a stronger effect of this variant on the overall phenotype. Our MD simulations also corroborate this idea, since the structural changes assessed from visual inspection of the MD trajectories were generally more predominant for the R178 mutants when compared with the others. However, since our analysis focused only on the whole protein or specific regions (as described in Tables 3–6), it is possible that we have missed subtle changes involving smaller sub-regions that might lead to significant local structural differences in functionally important domains. To further investigate and understand such changes, the crystal structure for each mutant protein should be determined and longer MD simulations (on the μs to ms scale) should be performed.

From our cohort of 11 MMIHS patients, 3 of them did not carry a variant in *ACTG2* (F1, F2 and F3). These patients were considered to be familial cases. Since a homozygous variant in *MYH11* (L1200 T) has been recently identified in a patient of consanguineous descent diagnosed with MMIHS and prune belly syndrome (15), we screened this gene in our familial cases. However, no variant was found in any of them (data not shown). The absence of *ACTG2* and *MYH11* variants in these patients strengthens the idea of locus heterogeneity and suggests the involvement of other genes in MMIHS pathogenesis. These genes would be associated to the familial cases, in which an autosomal recessive

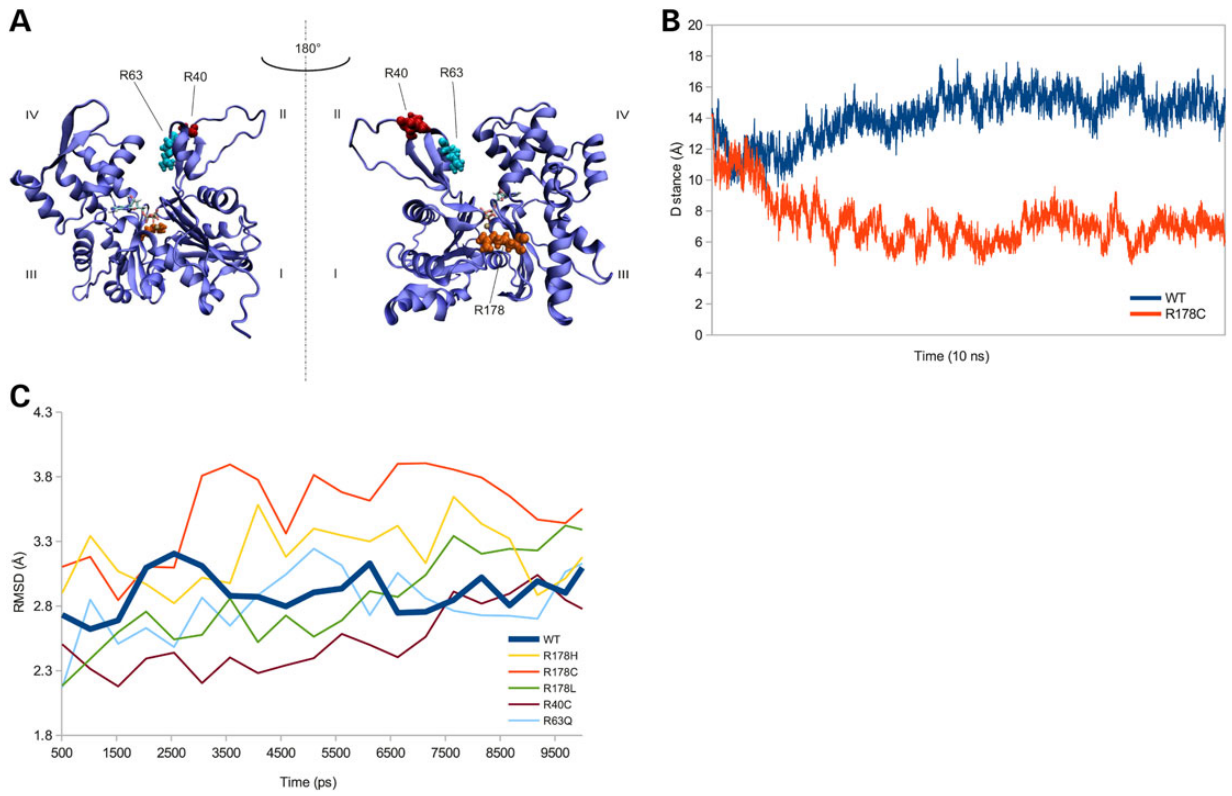

Figure 3. Molecular modeling and MD simulations of ACTG2 WT and mutant proteins. (**A**) Ribbon representation of the secondary structure of ACTG2. Residues of interest have been depicted as van der Waals' spheres. The representation on the bottom has been obtained by 180° rotation around the vertical axis. (**B**) RMSD of ACTG2 alpha-carbon trace (376 residues) for WT and mutant proteins plotted as a function of time every 0.5 ns. The behavior of each protein was analyzed every 50 ps. (**C**) Distance between Subdomains II and IV for ACTG2 WT and the R178C mutant shows significant differences over time. Distances were calculated between alpha-carbons of Thr67 (on Subdomain II) and Ala205 (on Subdomain IV).

pattern of inheritance is expected. Since our immunohistochemistry data show that ACTG2 localizes to the intestinal smooth muscle, and myosin and actin are two major proteins involved in muscle contractility, MMIHS can be considered to result from a myopathic defect. Therefore, we believe that particular attention should be paid to other proteins involved in the contractile apparatus, as impaired function of any of these proteins could also possibly lead to the same syndrome or overlapping clinical entities. Alternately, Filamin A (FLNA), an actin binding protein with a well-characterized role in the cytoplasm, could also be considered to be another suitable candidate for MMIHS, especially because of its known involvement in other intestinal motility disorders (25–27).

VM and MMIHS are clinically two separate disorders with overlapping features. The main differences rely on the age of onset, MMIHS can be diagnosed prenatally due to a recognizable bladder distension while VM occurs during adolescence, and disease severity with most MMIHS patients surviving only a few days or months after birth. The identification of *ACTG2* missense variants as the cause of both disorders led to their recent classification as ACTG2-related disorders, and suggested that MMIHS and VM could be one entity with a continuum of symptoms that vary in severity (28). To investigate this possibility, we included one of the VM missense variants previously described (R148S) (19), in our study, and analyzed its effect on the structure and function of ACTG2. Our MD simulations and *in vitro* results corroborated this idea, as the R148S variant affected ACTG2 structure and function in a similar way as the MMIHS variants. However, contradictory to what has been previously reported for VM patients carrying a R148S variant (19), we were unable to detect the presence of ACTG2 positive inclusions in any of the MMIHS patients analyzed by immunohistochemistry. We found instead a diffuse cytoplasmic distribution of ACTG2 (Fig. 2B). Considering that we were unable to obtain material from a VM patient carrying the R148S variant, we cannot rule out the possibility that the R148S variant leads to specific localization changes of ACTG2 that do not occur in the presence of the MMIHS-associated variants. However, based on our results, we have no indication that MMIHS and VM are pathophysiologically different disorders. We can only hypothesize that variants identified in MMIHS cause specific conformational changes that do not occur in VM, but disrupt binding of ACTG2 to key interactors required for intestinal and bladder development, accounting for a more severe phenotype in MMIHS.

Materials and Methods

Patient information

In this study, a cohort of 11 MMIHS patients was analyzed. Eight of these patients were sporadic cases (S1-S8), two patients were siblings of consanguineous descent (F1 and F2), and one patient was derived from an isolated Dutch community where inbreeding was suspected and was thus, considered as a familial case (F3). Patient S1 has been previously reported (29). Prenatal ultrasounds showed the presence of a distended bladder in the majority of the patients included in this study. A final MMIHS diagnosis was confirmed in all of them, due to the presence of a microcolon and distended bladder. All patients included in this study were Caucasian, except for Patients F1, F2 and F3 of North African ancestry. Written informed consent was given by the families, and ethical approval was obtained from the Erasmus Medical Center

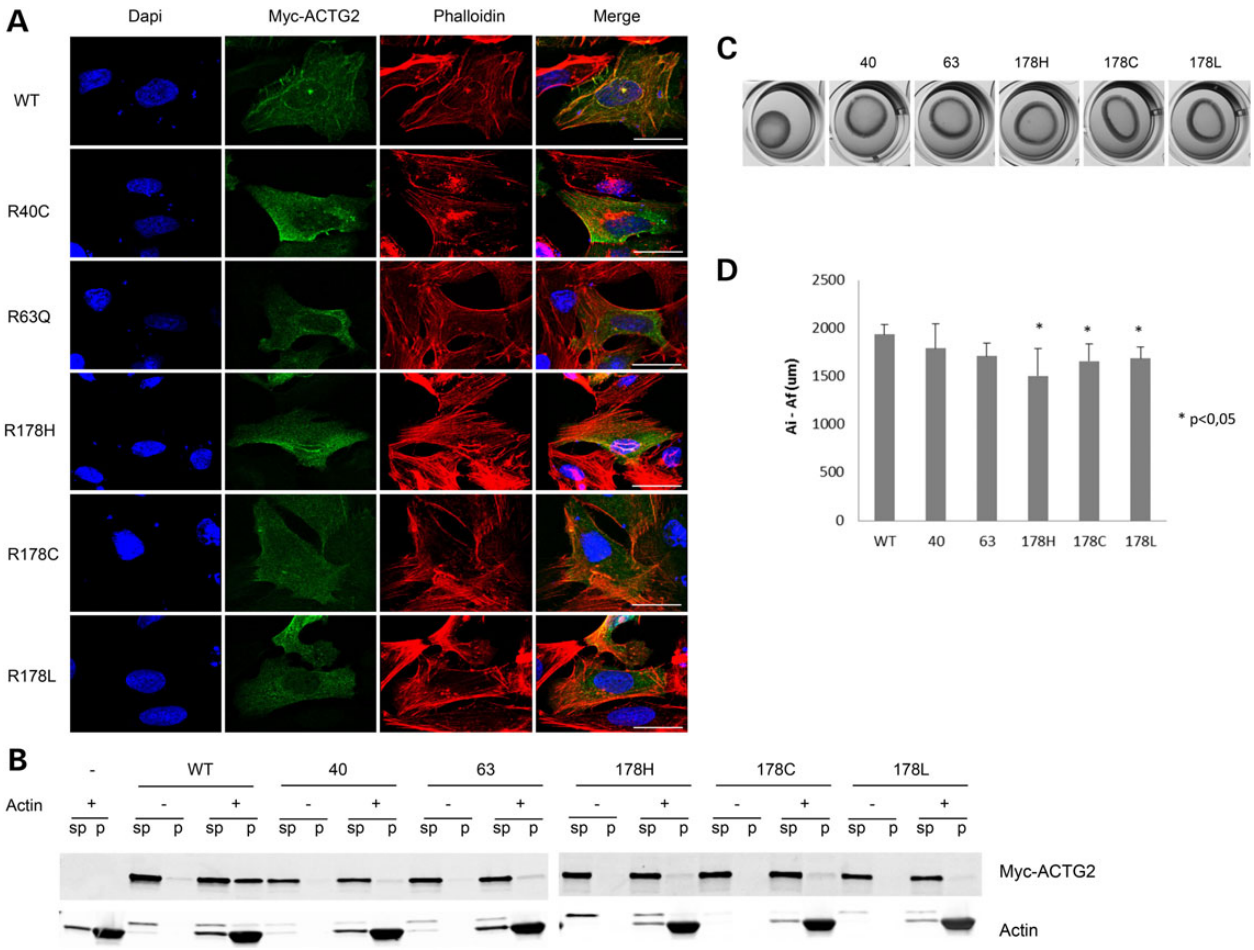

Figure 4. Cellular distribution and function of ACTG2 WT and mutant proteins. (**A**) Confocal images of U2OS cells stained for Phalloidin (a F-actin marker), and expressing a Myc-tagged version of ACTG2 WT and mutant proteins show reduced incorporation of the mutant proteins into the actin filaments. (**B**) *In vitro* actin binding assays show that ACTG2 mutant proteins do not precipitate with polymerized actin when subjected to high-speed centrifugation. (**C**) Contractility assays performed for ACTG2 WT and mutant proteins show a reduction in cellular contractility for all the mutants studied. (**D**) Quantification of the difference between the initial (0 h) and final (24 h) areas occupied by a collagen matrix confirms reduced cellular contractility for the mutant proteins. *($P < 0.05$); scale bars: 20 μm.

ethical committee (Medische Ethische Toetsings commissie—METc 2011/148, ABR form: NL35920.042.11).

Sanger sequencing

Genomic DNA was isolated from peripheral blood lymphocytes using standard methods. DNA obtained from amniotic fluid was extracted using standard DNA isolation protocols for prenatal material (Chemagic DNA Blood Kit Special, Chemagen, Perkin Elmer). Exons 1–10 of *ACTG2* were amplified using 15 ng of genomic DNA and the set of primers described in Supplementary Material, Table S1. PCR products were purified (ExoSap it – GE Healthcare), and Sanger sequencing was performed with dye labeled primers (forward and reverse; Big Dye Terminator v3.1 Sequencing Kit, Applied Biosystems) on an ABI 3130XL genetic analyzer. Sanger reads were analyzed using SeqScape software.

Immunohistochemistry

Fetal human gut tissues were obtained from the MRC-Wellcome Trust Human Developmental Biology Resource (HDBR), in collaboration with UCL Institute of Child Health in London, UK. Paraffin-embedded intestinal tissues from neonatal controls and Patients S3 and S5 were obtained from the Pathology Department repository of the Erasmus University Medical Center. Intestinal paraffin-embedded material from Patient S1 was obtained from Stanford Histology/EM Laboratory of the Stanford University Medical Center. All human embryonic and neonatal intestinal tissues used as control were obtained from elective abortions or from patients in which the cause of death was not intestinal related. Immunostainings were performed using specific antibodies against ACTG2 (1:100; Novus Biologicals), neurofilament (1:600; Monosan), smooth muscle actin α2 (ACTA2; ready to use; Dako), tyrosin protein kinase kit (c-Kit/CD117) (1:200; Cell Marque), tryptase (1:1600; Dako) and synaptophysin (SP11) (ready to use; Ventana). 3,3′-Diaminobenzidine (DAB) chromogen (Ventana) was used for protein visualization, and sections were counterstained with hematoxylin. All images were taken with the Nanozoomer 2.0-HT (Hamamatsu Photonics) and analyzed with the Nanozoomer Digital Pathology viewer software (Hamamatsu Photonics). Negative controls performed with depletion of primary antibody were included for each staining and showed no signal in any of the material tested (data not shown).

Molecular modeling and molecular dynamics simulations

MD simulations of ACTG2 were performed using the structure of the chicken actin gamma monomer in complex with Dnase1 (PDB

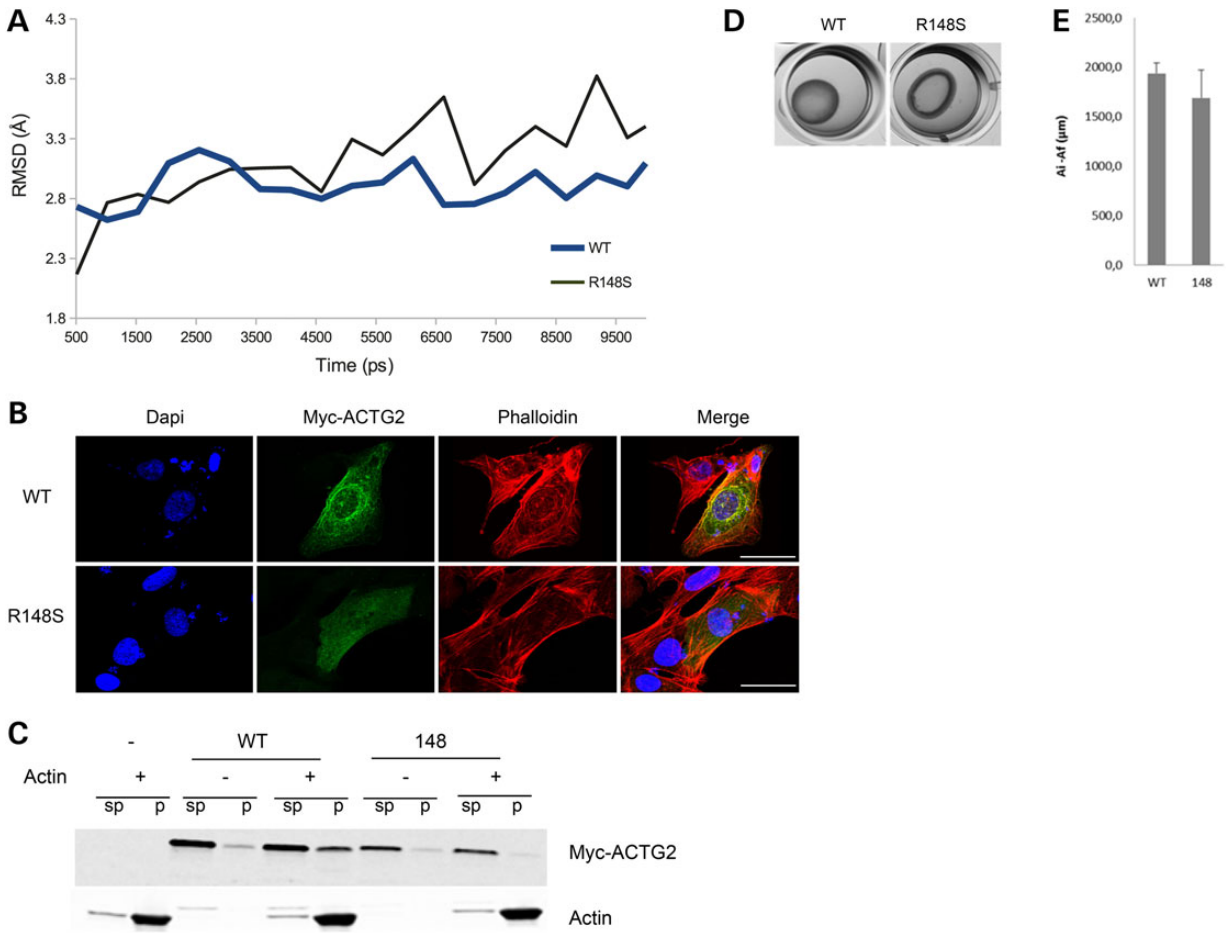

Figure 5. Effect of the R148S to the structure and function of ACTG2. (**A**) Molecular modeling and MD simulations of ACTG2 WT and the R148S mutant show moderate structural differences. (**B**) Confocal images of U2OS cells stained for Phalloidin (a F-actin marker), and expressing a Myc-tagged version of ACTG2 WT and of the R148S protein show reduced incorporation of the mutant into the actin filaments. (**C**) *In vitro* actin binding assays show that the R148S mutant protein does not precipitate with polymerized actin when subjected to high-speed centrifugation. (**D**) Contractility assays performed for ACTG2 WT and the R148S mutant protein show a reduction in cellular contractility for the mutant. (**E**) Quantification of the difference between the initial (0 h) and final (24 h) areas occupied by a collagen matrix confirms a reduced cell contractility for the R148S variant. However, this difference is not significant ($P > 0.05$). Scale bars: 20 µm.

ID: 3W3D) (30). In order to obtain only the actin subunit for subsequent MD simulations, removal of Dnase1, *N*-acetyl-D-glucosamine and alpha/beta-D-mannose structures was performed using the VMD software, version 1.9.1 (31). Different ACTG2 mutants were produced using the in-built VMD plugin 'mutate residue'. Each mutant was then checked for chirality errors and cis peptide bonds to ensure proper geometry via dedicated VMD plugins. An explicit 15 Å-padding TIP3P water box was used to solvate the protein, and the system was neutralized with KCl. All-atom MD simulations were performed with the NAMD software on a 32-core Intel® Xeon(R) CPU E5-2665 (32). Integration steps of 2 fs were used for minimization, equilibration and productive run in an isothermal–isobaric ensemble with a constant number of particles, pressure and temperature (NPT ensemble), in the presence of periodic boundary conditions (PBC) and Particle Mesh Ewalds (PME) for full electrostatics. The temperature of 310 K was ensured by Langevin dynamics with a damping coefficient of 2 ps, and pressure was maintained constant at 1.013 bar by a Langevin Piston. Minimization was performed for 20 ps and productive run for 10 ns. Simulations were performed using the same parameters for mutants and WT. Analysis was carried out with standard VMD Analysis tools. RMSD was calculated over the alpha-carbon traces every 50 ps.

Expression vectors

pCMV6-Myc-ACTG2 WT was purchased from Origene. All the mutants described were generated by site-directed mutagenesis on pCMV6-Myc-ACTG2 WT according to the manufacturer's instructions (QuickChange II site-directed mutagenesis kit, Agilent technologies). Primers used are listed in Supplementary Material, Table S2. Following mutagenesis, the entire ACTG2 insert was checked by Sanger sequencing.

Cell culture and transfection

The U2OS cell line was cultured in DMEM with high glucose content (Lonza), supplemented with 10% fetal calf serum (Sigma-Aldrich) and 1% penicillin/streptomycin (Gibco). Cells were maintained at 37°C and 5% CO_2. For transient transfection, 300 000 cells were seeded in 6-well plates. Transfection was performed 24 h after using GeneJuice transfection reagent (Millipore) according to the manufacturer's instructions.

Cell lysates and western blot analysis

Cells were washed with PBS and incubated with lysis buffer [m-PER (Thermo Scientific) containing protease inhibitors (Roche)],

for 30 min on ice. Cell lysates were collected by scraping and cleared by centrifugation at 14 000 rpm for 10 min in a pre-cooled (4°C) centrifuge. Lysates were stored at −80°C before being processed further for SDS-PAGE and immunoblotting. Protein quantification was performed using a BCA kit (Thermo Scientific), and 30 μg of protein was loaded into a criterion TGX precast gel (Bio-Rad). The following antibodies were used: Myc (Cell Signaling) and GAPDH (Millipore). Secondary antibodies used were IRDye 800CW goat anti-mouse and IRDye 680RD goat anti-rabbit (Li-Cor).

Microscopy and image analysis

For immunofluorescence, cells were cultured on cover slips. Four percent paraformaldehyde was used as a fixative, and cells were permeabilized with 1% BSA and 0.1% Triton X-100 in PBS. Myc antibody (Cell Signaling) was used at a concentration of 1:100, and Phalloidin-rhodamin (Santa Cruz Biotechnology) was used at a concentration of 1:500. Images were taken using a Leica (AOBS) microscope, and analyzed with the Leica LAS AF Lite software.

Actin binding assays

U2OS cells transfected with ACTG2 expressing constructs (WT and mutants) were lysed in an actin buffer (Cytoskeleton) containing 0.1% Triton X-100 (Sigma) and protease inhibitors (Roche). Lysates were centrifuged for 15 min at 14 000 rpm in a pre-cooled centrifuge (4°C), and supernatant fractions were incubated with polymerized actin (F-actin), generated according to the manufacturer's instructions (Cytoskeleton™). Polymerized actin was pelleted by centrifugation (100 000 G for 1 h) using the Airfuge, Air-driven Ultracentrifuge (Beckman-Coulter). Supernatant and pellet fractions were further analyzed by western blotting.

Contractility assays

Twenty-four hours after transfection with ACTG2 expressing constructs (WT and mutants), U2OS cells were trypsinized, and analyzed for their ability to contract. A cell contraction kit (Cell Biolabs) was used according to the manufacturer's instructions.

Supplementary Material

Supplementary Material is available at *HMG* online.

Acknowledgements

The authors would like to thank all the patients and families involved in this study. The authors would also like to thank Prof. Henny van der Mei for providing the U2OS cell line, J. A. Stoop for technical assistance with the immunohistochemistry work and Kaushal Parikh for critically reviewing the manuscript.

Conflict of Interest statement: None declared.

Funding

This work was supported by the Stichting Sophia Kinderziekenhuis Fonds (R.M.W.H. and M.M.A.), the Erasmus TrustFonds (D.H. and M.M.A.) and the Top subsidy (R.M.W.H.).

References

1. Berdon, W.E., Baker, D.H., Blanc, W.A., Gay, B., Santulli, T.V. and Donovan, C. (1976) Megacystis-microcolon-intestinal hypoperistalsis syndrome: a new cause of intestinal obstruction in the newborn. Report of radiologic findings in five newborn girls. *AJR Am. J. Roentgenol.*, **126**, 957–964.
2. Ciftci, A.O., Cook, R.C. and van Velzen, D. (1996) Megacystis microcolon intestinal hypoperistalsis syndrome: evidence of a primary myocellular defect of contractile fiber synthesis. *J. Pediatr. Surg.*, **31**, 1706–1711.
3. Rolle, U., O'Briain, S., Pearl, R.H. and Puri, P. (2002) Megacystis-microcolon-intestinal hypoperistalsis syndrome: evidence of intestinal myopathy. *Pediatr. Surg. Int.*, **18**, 2–5.
4. Szigeti, R., Chumpitazi, B.P., Finegold, M.J., Ranganathan, S., Craigen, W.J., Carter, B.A. and Tatevian, N. (2010) Absent smooth muscle actin immunoreactivity of the small bowel muscularis propria circular layer in association with chromosome 15q11 deletion in megacystis-microcolon-intestinal hypoperistalsis syndrome. *Pediatr. Dev. Pathol.*, **13**, 322–325.
5. Narayanan, M., Murphy, M.S., Ainsworth, J.R. and Arul, G.S. (2007) Mydriasis in association with MMIHS in a female infant: evidence for involvement of the neuronal nicotinic acetylcholine receptor. *J. Pediatr. Surg.*, **42**, 1288–1290.
6. Richardson, C.E., Morgan, J.M., Jasani, B., Green, J.T., Rhodes, J., Williams, G.T., Lindstrom, J., Wonnacott, S., Thomas, G.A. and Smith, V. (2001) Megacystis-microcolon-intestinal hypoperistalsis syndrome and the absence of the alpha3 nicotinic acetylcholine receptor subunit. *Gastroenterology*, **121**, 350–357.
7. Kubota, M., Ikeda, K. and Ito, Y. (1989) Autonomic innervation of the intestine from a baby with megacystis microcolon intestinal hypoperistalsis syndrome: II. Electrophysiological study. *J. Pediatr. Surg.*, **24**, 1267–1270.
8. Piaseczna Piotrowska, A., Rolle, U., Solari, V., Solari, V. and Puri, P. (2004) Interstitial cells of Cajal in the human normal urinary bladder and in the bladder of patients with megacystis-microcolon intestinal hypoperistalsis syndrome. *BJU Int.*, **94**, 143–146.
9. Piotrowska, A.P., Rolle, U., Chertin, B., De Caluwé, D., Bianchi, A. and Puri, P. (2003) Alterations in smooth muscle contractile and cytoskeleton proteins and interstitial cells of Cajal in megacystis microcolon intestinal hypoperistalsis syndrome. *J. Pediatr. Surg.*, **38**, 749–755.
10. Anneren, G., Meurling, S. and Olsen, L. (1991) Megacystis-microcolon-intestinal hypoperistalsis syndrome (MMIHS), an autosomal recessive disorder: clinical reports and review of the literature. *Am. J. Med. Genet.*, **41**, 251–254.
11. Mc Laughlin, D. and Puri, P. (2013) Familial megacystis microcolon intestinal hypoperistalsis syndrome: a systematic review. *Pediatr. Surg. Int.*, **29**, 947–951.
12. Thorson, W., Diaz-Horta, O., Foster, J., Spiliopoulos, M., Quintero, R., Farooq, A., Blanton, S. and Tekin, M. (2014) De novo ACTG2 mutations cause congenital distended bladder, microcolon, and intestinal hypoperistalsis. *Hum. Genet.*, **133**, 737–742.
13. Wangler, M.F., Gonzaga-Jauregui, C., Gambin, T., Penney, S., Moss, T., Chopra, A., Probst, F.J., Xia, F., Yang, Y., Werlin, S. *et al.* (2014) Heterozygous de novo and inherited mutations in the smooth muscle actin (ACTG2) gene underlie megacystis-microcolon-intestinal hypoperistalsis syndrome. *PLoS Genet.*, **10**, e1004258.
14. Tuzovic, L., Tang, S., Miller, R.S., Rohena, L., Shahmirzadi, L., Gonzalez, K., Li, X., LeDuc, C.A., Guo, J., Wilson, A. *et al.* (2015)

New insights into the genetics of fetal megacystis: ACTG2 mutations, encoding γ-2 smooth muscle actin in megacystis microcolon intestinal hypoperistalsis syndrome (Berdon syndrome). *Fetal Diagn. Ther.*, **38**, 296–306.
15. Gauthier, J., Ouled Amar Bencheikh, B., Hamdan, F.F., Harrison, S.M., Baker, L.A., Couture, F., Thiffault, I., Ouazzani, R., Samuels, M.E., Mitchell, G.A. *et al.* (2014) A homozygous loss-of-function variant in MYH11 in a case with megacystis-microcolon-intestinal hypoperistalsis syndrome. *Eur. J. Hum. Genet.*, **23**, 1266–1268.
16. Miwa, T., Manabe, Y., Kurokawa, K., Kamada, S., Kanda, N., Bruns, G., Ueyama, H. and Kakunaga, T. (1991) Structure, chromosome location, and expression of the human smooth muscle (enteric type) gamma-actin gene: evolution of six human actin genes. *Mol. Cell Biol.*, **11**, 3296–3306.
17. Szucsik, J.C. and Lessard, J.L. (1995) Cloning and sequence analysis of the mouse smooth muscle gamma-enteric actin gene. *Genomics*, **28**, 154–162.
18. Morano, I., Chai, G.X., Baltas, L.G., Lamounier-Zepter, V., Lutsch, G., Kott, M., Haase, H. and Bader, M. (2000) Smooth-muscle contraction without smooth-muscle myosin. *Nat. Cell Biol.*, **2**, 371–375.
19. Lehtonen, H.J., Sipponen, T., Tojkander, S., Karikoski, R., Järvinen, H., Laing, N.G., Lappalainen, P., Aaltonen, L.A. and Tuupanen, S. (2012) Segregation of a missense variant in enteric smooth muscle actin gamma-2 with autosomal dominant familial visceral myopathy. *Gastroenterology*, **143**, 1482–1491.
20. Holla, O.L., Bock, G., Busk, O.L. and Isfoss, B.L. (2014) Familial visceral myopathy diagnosed by exome sequencing of a patient with chronic intestinal pseudo-obstruction. *Endoscopy*, **46**, 533–537.
21. Klar, J., Raykova, D., Gustafson, E., Tóthová, I., Ameur, A., Wanders, A. and Dahl, N. (2015) Phenotypic expansion of visceral myopathy associated with ACTG2 tandem base substitution. *Eur. J. Hum. Genet.*, **23**, 1679–1683.
22. Arnoldi, R., Hiltbrunner, A., Dugina, V., Tille, J.C. and Chaponnier, C. (2013) Smooth muscle actin isoforms: a tug of war between contraction and compliance. *Eur. J. Cell Biol.*, **92**, 187–200.
23. Milewicz, D.M., Østergaard, J.R., Ala-Kokko, L.M., Khan, N., Grange, D.K., Mendoza-Londono, R., Bradley, T.J., Olney, A. H., Adès, L., Maher, J.F. *et al.* (2010) De novo ACTA2 mutation causes a novel syndrome of multisystemic smooth muscle dysfunction. *Am J. Med. Genet.*, **152**, 2437–2443.
24. Richer, J., Milewicz, D.M., Gow, R., de Nanassy, J., Maharajh, G., Miller, E., Oppenheimer, L., Weiler, G. and O'Connor, M. (2012) R179H mutation in ACTA2 expanding the phenotype to include prune-belly sequence and skin manifestations. *Am. J. Med. Genet. A*, **158A**, 664–668.
25. Gargiulo, A., Auricchio, R., Barone, M.V., Cotugno, G., Reardon, W., Milla, P.J., Ballabio, A., Ciccodicola, A. and Auricchio, A. (2007) Filamin A is mutated in X-linked chronic idiopathic intestinal pseudo-obstruction with central nervous system involvement. *Am. J. Hum. Genet.*, **80**, 751–758.
26. Clayton-Smith, J., Walters, S., Hobson, E., Burkitt-Wright, E., Smith, R., Toutain, A., Amiel, J., Lyonnet, S., Mansour, S., Fitzpatrick, D. *et al.* (2008) Xq28 duplication presenting with intestinal and bladder dysfunction and a distinctive facial appearance. *Eur. J. Hum. Genet.*, **17**, 434–443.
27. Kapur, R.P., Robertson, S.P., Hannibal, M.C., Finn, L.S., Morgan, T., van Kogelenberg, M. and Loren, D.J. (2010) Diffuse abnormal layering of small intestinal smooth muscle is present in patients with FLNA mutations and x-linked intestinal pseudo-obstruction. *Am. J. Surg. Pathol.*, **34**, 1528–1543.
28. Wangler, M.F. and Beaudet, A.L. (2015) ACTG2-related disorders. GeneReviews® [Internet]. Seattle (WA): University of Washington, Seattle; 1993–2015. In: Pagon, R.A., Adam, M.P., Ardinger, H.H., Wallace, S.E., Amemiya, A., Bean, L.J.H., Bird, T.D., Fong, C.T., Smith, R.J.H. and Stephens, K., editors.
29. Talisetti, A., Longacre, T., Pai, R.K. and Kerner, J. (2009) Diversion colitis in a 19-year-old female with megacystis-microcolon-intestinal hypoperistalsis syndrome. *Dig. Dis. Sci.*, **54**, 2338–2340.
30. Sasaki, K., Sakabe, K., Sakabe, N., Kondo, H. and Shimomur, M. (1993) Refined structure and solvent network of chicken gizzard G-actin DNase 1 complex at 1.8A resolution. *Acta Crystallogr. Sect. A*, **49**, C111–C112.
31. Humphrey, W., Dalke, A. and Schulten, K. (1996) VMD - visual molecular dynamics. *J. Molec. Graphics*, **14**, 33–38.
32. Phillips, J.C., Braun, R., Wang, W., Gumbart, J., Tajkhorshid, E., Villa, E., Chipot, C., Skeel, R.D., Kalé, L. and Schulten, K. (2005) Scalable molecular dynamics with NAMD. *J. Comput. Chem.*, **26**, 1781–1802.